




DECEMBER 07 2023

Effect of streamwise vane treatments on the noise reduction performance of trailing edge serrations under aerodynamic loading conditions ✓

Shivam Sundeep  ; Peng Zhou  ; Siyang Zhong 



J. Acoust. Soc. Am. 154, 3684–3695 (2023)

<https://doi.org/10.1121/10.0022579>



Articles You May Be Interested In

Aeroacoustic design and broadband noise predictions of a fan stage with serrated outlet guide vanes

Physics of Fluids (October 2020)

An experimental investigation of aerodynamic and aeroacoustic performance of a wind turbine airfoil with trailing edge serrations

J. Acoust. Soc. Am. (February 2022)

On the use of leading-edge serrations for noise control in a tandem airfoil configuration




Physics of Fluids (July 2020)



LEARN MORE

Advance your science and career as a member of the
Acoustical Society of America

Effect of streamwise vane treatments on the noise reduction performance of trailing edge serrations under aerodynamic loading conditions

Shivam Sundee¹  Peng Zhou,^{1,a)}  and Siyang Zhong² 

¹Department of Mechanical and Aerospace Engineering, The Hong Kong University of Science and Technology, Clear Water Bay, Kowloon, Hong Kong Special Administrative Region, China

²Department of Aeronautical and Aviation Engineering, The Hong Kong Polytechnic University, Hung Hom, Kowloon, Hong Kong Special Administrative Region, China

ABSTRACT:

Trailing edge serrations have shown remarkable ability to reduce noise, but their effectiveness can be significantly impacted by flow misalignment, particularly under aerodynamic loading conditions. This paper presents a comprehensive study on the effect of incorporating streamwise vane treatments at the root of the trailing edge serrations on its noise reduction performance. Experiments were performed on a 100 mm chord NACA 0012 wing model with sawtooth type trailing edge serration. The aeroacoustic performance was investigated for serrations with non-zero flap angle at various angles of attack between -5° and 8.5° . The findings reveal that streamwise vanes can reduce the high-frequency noise by over 5 dB when placed at the root. Furthermore, particle image velocimetry measurements in the wall-normal plane demonstrate a significant decrease in cross-flow and turbulence generation when the treatment was placed near the root of serrations. In addition, the load measurements indicate no noticeable variation in the lift coefficient and up to 6% increase in the drag coefficients in the pre-stall region.

© 2023 Acoustical Society of America. <https://doi.org/10.1121/10.0022579>

(Received 28 July 2023; revised 3 November 2023; accepted 13 November 2023; published online 7 December 2023)

[Editor: Xun Huang]

Pages: 3684–3695

I. INTRODUCTION

Over the past two decades, there has been a notable increase in the size of wind turbines, with their height and blade lengths growing significantly, to enhance their energy generation capabilities. Larger blade diameter enables wind turbine to sweep more area, capture more wind, and produce more electricity. However, the wind turbine blades also cause high noise pollution, leading to development of high-loading, low-noise blades. Researchers have drawn inspiration from the exceptional low-noise flight abilities of owls to investigate noise reduction techniques such as trailing edge serrations,¹ porous membranes and airfoils,^{2,3} finlets,^{4,5} and canopies.⁶

Presently, sawtooth type trailing edge serration is a preferred method for reducing the wind turbine trailing edge turbulent boundary layer interaction noise.⁷ The wind tunnel experiments by Gruber *et al.*¹ and Oerlemans *et al.*⁸ have illustrated that the serrated trailing edge inserts can achieve a noise reduction of up to 6 dB. However, they also reported an increase in noise at relatively higher frequencies. Gruber *et al.*¹ suggested that this increase in noise at higher frequencies might be attributed to heightened turbulence activity occurring between the serration teeth. Avallone *et al.*⁹ employed time-resolved tomographic particle image

velocimetry (PIV) to directly visualise the three-dimensional (3D) flow patterns over the suction side of a NACA 0018 airfoil equipped with trailing-edge serrations. Their findings revealed the presence of pairs of counter-rotating vortices aligned along the streamwise direction within the spaces between the serrations. These vortical structures were driven by the mean pressure difference between the suction and pressure sides of the airfoil. Based on the flow visualisation using active liquid crystals and surface pressure sensors, Chong and Vathylakis¹⁰ suggested that the reduction in noise in serrations is attributed to a decline in scattering efficiency caused by oblique edges, rather than a reduction in the strength of the noise source.

Recent experimental and numerical studies^{11–15} have found that the noise reduction performance of serrations is sensitive to the installation and loading conditions. It has been shown that even minor changes in incidence can make the flow more complex and three-dimensional and, hence, deduce the noise reduction capability of serration. Arce León *et al.*¹¹ used PIV measurements to examine the effects of loading and flap angle on the cross-flow across the serration roots. They observed pairs of counter-rotating vortices between the serrations as a result of the pressure imbalance across the serration edges. These vortices significantly alter the streamline pattern and affect the surface pressure fluctuations and acoustic scattering efficiency. They concluded that the formulation presented by Howe,¹⁶ which only

^{a)}Email: pengzhou@ust.hk

considers the sideward deviation of streamlines relative to the serration edge, is insufficient to account for the observed variations in noise reduction.

Later, Vathylakis *et al.*¹² and Woodhead *et al.*¹⁵ expanded upon the study and investigated the impact of both flap-up and flap-down serrations. Their research revealed that while the flap-up position is more favourable for broadband noise reduction, it has a negative impact on lift. Conversely, the flap-down configuration has the opposite effect. Recently, Pereira *et al.*¹⁷ provided a comprehensive analysis of the surface pressure fluctuations over serrations impacted by the cross-flow around the serrated trailing edge subjected to aerodynamic loading. Their findings revealed that the streamwise vortices cause the flow to steer towards the centre of the serration on the suction side and towards the gap on the pressure side, resulting in amplified pressure fluctuations around the edges on the pressure side.

Although numerous studies have examined the adverse effects of cross-flow on noise reduction, there has been relatively little research focused on minimizing it. In a previous study,¹⁸ the authors successfully reduced the cross-flow by shifting the serrations downstream of the airfoil trailing edge. Shi and Kollmann¹⁹ numerically investigated the combination of trailing edge serrations and upstream finlet structures, which were originally used to mitigate broadband trailing edge noise.^{4,20} Their results showed a significant noise reduction in the entire frequency range. However, the highly separated flow in their baseline case was not a representative condition from a practical perspective. This study aims to improve the noise reduction performance of trailing edge serrations by suppressing the cross-flow across trailing edge serration by placing streamwise vanes upstream of the root of the serrations in a staggered arrangement. While this arrangement has similarities to the staggered finlets used by Afshari *et al.*,²⁰ they differ in placement, coverage, and function. Specifically, unlike finlets, the vanes are intermittently placed around the edge of serrations and cover only 20% of the total span. The design purpose of the vanes is to block the cross-flow and reduce the strength of streamwise vortices from the serration roots, instead of elevating the boundary layer, which is a key function of finlets.²⁰ This study includes comprehensive anechoic wind tunnel measurements to provide better understanding of the aerodynamic and aeroacoustic effects of the streamwise vane treatments across a broad range of angles of attack.

The remainder of this paper is structured as follows. Section II outlines the experimental setup and the instrumentations used in this study. In Sec. III, the results of the aeroacoustic and aerodynamic measurements are presented, with an insight into the noise reduction mechanism. Finally, Sec. IV provides concluding remarks on the study.

II. EXPERIMENTAL SETUP

A. Wind tunnel and flow conditions

Experiments were carried out in a low-speed wind tunnel the Ultra-quiet Noise Injection Test and Evaluation Device

(UNITED),²¹ at the Hong Kong University of Science and Technology (HKUST). The wind tunnel has an open-jet test section with a square nozzle of 0.4 m each side at the exit. The test section was enclosed by an anechoic chamber with a cut-off frequency of around 200 Hz. The wind tunnel has a turbulent intensity of less than 0.25% over the whole operating range. A NACA 0012 wing model²² with a span of 0.4 m and a chord (c) of 0.1 m was used for the study. The wing was positioned between two end plates in an open-jet test section, as shown in Fig. 1. The boundary layer transition was forced at $0.15c$ on both the pressure and suction sides of the wing by means of a 0.2 mm thick zig-zag trip. The experiments were conducted at free stream velocities ranging from 20 m/s to 50 m/s, corresponding to chord-based Reynolds numbers ranging from 1.38×10^5 to 3.45×10^5 .

The wing model was attached to a turntable (Fig. 1) with a stepper motor and an optical encoder to precisely control the angle of attack, with an accuracy of 0.01° . Acoustic measurements were conducted at four different geometric angles of attack: $\alpha_g = -7^\circ, 0^\circ, 7^\circ$, and 12° . To determine the effective angle of attack, the correction methodology proposed by Brooks *et al.*²³ was utilised: $\alpha = \alpha_g(1 + 2\sigma)/\eta$, where $\eta = (1 + 2\sigma)^2\sqrt{12\sigma}$, $\sigma = (\pi^2/48)(c/L)^2$, and $L = 0.4$ m; is the height of the nozzle. The corresponding effective angles of attack are $\alpha = -5^\circ, 0^\circ, 5^\circ$, and 8.5° , respectively.

1. Trailing edge serration and streamwise vane treatment

The serrations have a sawtooth profile with a wavelength of $\lambda = 10$ mm and a root-to-tip distance of $2h = 20$ mm. The serrations were treated by streamwise vanes at its roots. Both the serrations and the streamwise vanes were 3D printed as a single entity from Nylon PA12 material. The streamwise vanes and the substrate have thicknesses of 0.3 mm and 0.2 mm, respectively, with a dimensional accuracy of $\pm 5\%$. Following fabrication, these serrations along with the

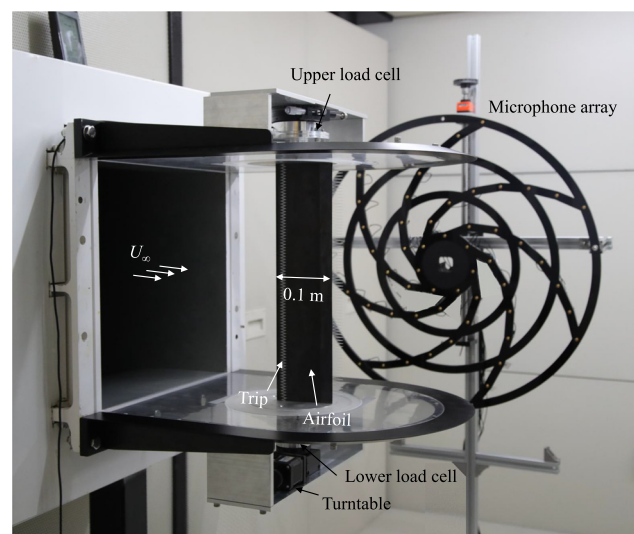


FIG. 1. (Color online) An overview of the experimental setup.

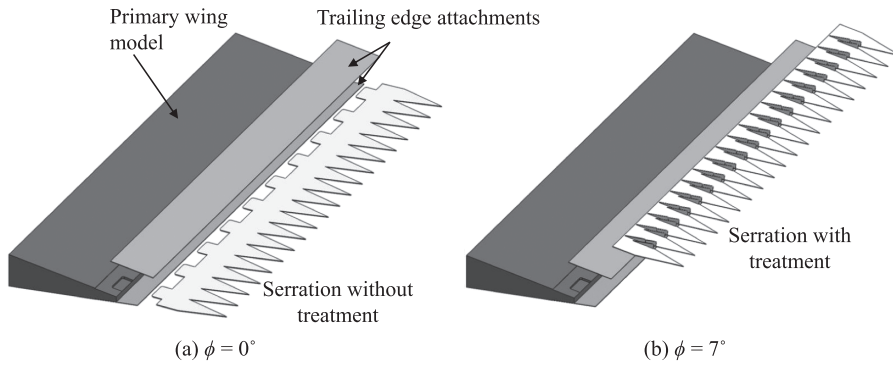


FIG. 2. Trailing edge attachment of the wing model to obtain different serration flap angles.

streamwise vanes were placed at the trailing edge of the wing using trailing edge attachments, as shown in Fig. 2. These attachments are 0.1 mm thin stainless steel strips attached to the wing using magnets to allow easy replaceability. After assembly, the thickness of the trailing edge adds up to 0.4 mm, corresponding to $t/\delta^* = 1.33$, where δ^* is the displacement thickness at the trailing edge. Although this value falls in the vortex shedding limit of $t/\delta^* > 0.25$ suggested by Blake,²⁴ the vortex shedding effect was too small to be observed in the acoustic spectra, as shown in Sec. III A 1.

Moreover, the trailing edge add-ons offer the flexibility of placing serrations at either a 0° or 7° flap angle (ϕ), as shown in Fig. 2. For a 0° flap angle, the serrations can be inserted into the slots between the add-ons, whereas for a 7° flap angle, the serrations are affixed on top of the add-ons using adhesive. Due to the design constraints, it was only possible to test the treatments on the suction side and at a 7° flap angle.

The streamwise vanes were arranged in a staggered configuration at the root of the serration such that they make contact with its edges, as depicted in Fig. 3. The root of the serration was set as the origin. The x axis is aligned along the direction of the main flow, the y axis is aligned in the chord-normal direction, and the z axis represents the spanwise direction. Through a parametric study, optimal treatment parameters for minimising serration noise were determined and were chosen as a baseline for the detailed investigation. The outcome of this parametric study is provided in the Appendix. The nomenclature and parameters of

various streamwise vanes used in the study are given in Table I. Furthermore, the optimal location for the vanes' placement was also tested by placing them at different positions along the serration edges, as shown in Fig. 4. Four different test cases with vanes placed at root, mid, tip and full serration were compared for this study. For the treatment at root case, the rear vane's leading edge is positioned 0.5 mm behind the serration's root. In the case of the treatment at mid, the leading edge of the rear vanes is located at 25% of the root-to-tip distance ($2h$) from the root of the serration. Similarly, in the case of treatment at tip, the leading edge of the rear vanes is situated at 50% of the root-to-tip distance ($2h$) from the root of the serration. The full serration case represents a combination of the other three cases.

B. Acoustic measurements

Acoustic measurements were conducted using a phased microphone array consisting of $56\frac{1}{4}$ in. Brüel & Kjaer (Naerum, Denmark) type 4957 microphones, positioned 0.75 m away from the wing and parallel to the flow. The array acquired 100 blocks of 4096 samples at a sampling frequency of 48 kHz, which were then divided into 199 Hanning windows with a window size of 4096 and a 50% overlap, providing a frequency resolution of 11.72 Hz. The conventional frequency-domain beamforming technique²⁵ was used to obtain source maps. The sound source intensities were integrated within a $\frac{1}{4}$ span \times $\frac{3}{2}$ chord area centred around the trailing edge to obtain the sound pressure levels.²⁶ This approach was found to perform well for distributed sound sources, such as trailing edge noise.²⁷ An array

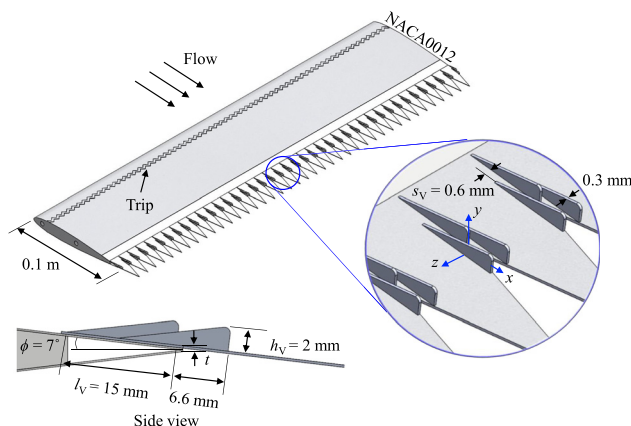


FIG. 3. (Color online) Schematic of the serrated trailing edge with the baseline C0 treatment.

TABLE I. List of streamwise vanes cases used for the parametric study, where δ is the boundary layer thickness at the trailing edge at 20 m/s.

| Description | Config. | h_v (mm) | h_v/δ | l_v (mm) | s_v (mm) | Position |
|-----------------------|---------|------------|--------------|------------|------------|----------|
| Baseline | C0 | 2 | 0.46 | 15 | 0.6 | Root |
| Variation in height | C1 | 1 | 0.23 | 15 | 0.6 | Root |
| | C2 | 4 | 0.92 | 15 | 0.6 | Root |
| Variation in length | C3 | 2 | 0.46 | 10 | 0.6 | Root |
| | C4 | 2 | 0.46 | 12.5 | 0.6 | Root |
| Variation in spacing | C5 | 2 | 0.46 | 15 | 0.8 | Root |
| | C6 | 2 | 0.46 | 15 | 1.2 | Root |
| Variation in position | C7 | 2 | 0.46 | 10 | 0.6 | Mid |
| | C8 | 2 | 0.46 | 10 | 0.6 | Tip |
| | C9 | 2 | 0.46 | 10 | 0.6 | Full |

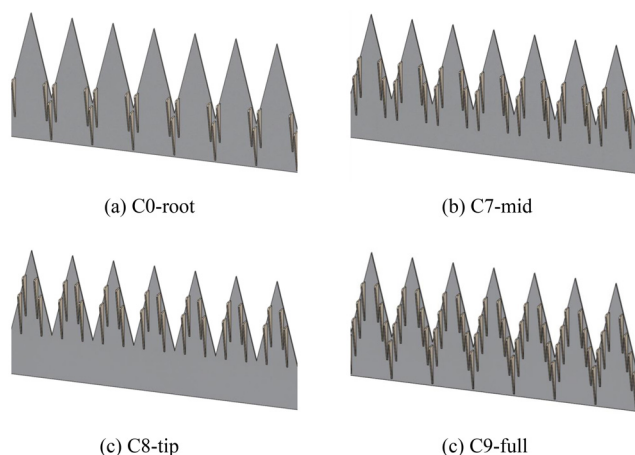


FIG. 4. (Color online) Schematic of treatments covering various extent of the serration.

calibration function based on simulated incoherent point sources was applied to convert the integrated result to equivalent far-field noise at the array centre. The final outcome was an equivalent sound spectrum measured by a single microphone located at the centre of the array. The analysis is explained in detail in Zhou *et al.*²⁸

C. Flow measurements

1. Hotwire measurements

A Dantec (Moreton, United Kingdom) 55P61 X-wire probe was used to simultaneously measure two velocity components in the cross-flow plane, as shown in Fig. 5. The probe was positioned at a distance of 1 mm downstream of the serration tip ($x/2h = 1.05$) and traversed in the cross-flow plane, covering a width of 6 mm (0.6λ) and span of 22 mm (2.2λ). The measurement array was discretised into 368 measurement points, with a spacing of 0.5 mm in both directions. At each location, the streamwise and wall-normal component of velocity was measured at a sampling frequency of 20 kHz for 10 s. The flow field was measured for the serrated trailing edge with and without treatment C0 at 30 m/s and $\alpha_g = 0^\circ$.

2. PIV measurements

In addition to the cross-flow measurements using the hotwire, measurements of the flow from the root the serration were taken using two-component particle image velocimetry (2D-2C PIV). The flow was seeded with diethylhexyl-sebacate (DEHS) droplets with a mean diameter of $1\ \mu\text{m}$. A dual cavity Nd-YLF laser sheet with a wavelength of 527 nm and energy output of 20 mJ was used to illuminate the flow. The laser sheet was 1 mm thick and was positioned along the root of the serration, as shown in Fig. 5. A charge-coupled device (CCD) camera equipped with a Nikon (Tokyo, Japan) Micro-Nikkor 200 mm prime lens and a sensor resolution of 1280×800 pixels was used to capture the images, resulting in a pixel resolution of 0.04 mm/pixel. The PIV images were processed using a multi-pass FFT cross correlation algorithm²⁹ with a final interrogation window of 32×32 pixels

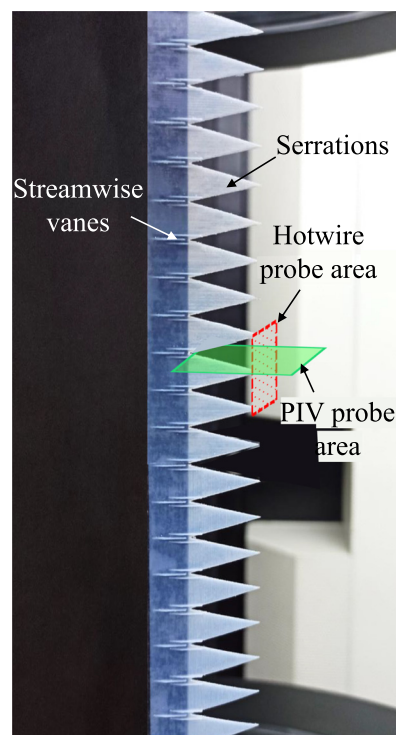


FIG. 5. (Color online) A side image of the streamwise vanes placed at the root of the serration along with the hotwire and PIV probe area.

and 50% overlap to determine the displacement of the average particle within the interrogation window.

D. Lift and drag measurements

The aerodynamic lift and drag by the wing were measured using load cells located at each end of the wing, as illustrated in Fig. 1. The top load cell was connected to a bearing, which allowed the wing to rotate freely, while the lower load cell was affixed to the turntable, which was used to vary the angle of attack. The load cells had a range of 40 N and a resolution of 0.01 N in both the chordwise and normal directions to the wing. The forces were recorded at a sampling frequency of 5 kHz for 10 s. Based on the five repeated measurements, the mean levels of uncertainty in the lift and drag coefficients are estimated as 0.005 and 0.001, respectively, which are equivalent to 1.25% and 2% of the respective values at $\alpha = 5^\circ$, with a 95% confidence level using the t distribution.

III. RESULTS AND DISCUSSION

A. Acoustics

The sound source spectra for various trailing edge configurations were obtained using beamforming. In Fig. 6, a comparison is made between the one-third octave trailing edge noise spectra for the serrated and straight trailing edge configurations at $\alpha = 0^\circ$. The flow aligned ($\phi = 0^\circ$) serration effectively reduces the high-frequency noise by up to 10 dB. At $\phi = 7^\circ$ flap angle, the serration performance deteriorates substantially, to the extent that the serrated trailing

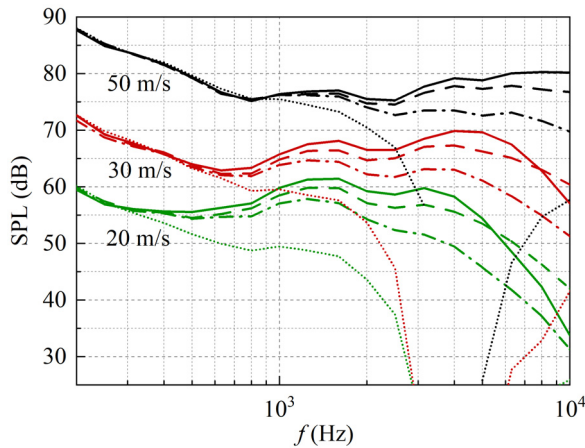


FIG. 6. (Color online) One-third octave trailing edge noise spectra at $\alpha = 0^\circ$ for different configurations: straight (solid line), serrated with flap angle of $\phi = 0^\circ$ (dashed-dotted line) and $\phi = 7^\circ$ (dashed line), and the background noise (dotted line).

edge noise becomes higher than the straight edge noise at higher frequencies. This observation is consistent with previous findings by Gruber *et al.*¹ and is attributed to the flow modifications induced by the serrations under flow-misalignment.

1. Baseline treatment, C0

This section highlights the effect of the baseline streamwise vanes placed at the root of the flapped serration

($\phi = 7^\circ$). Acoustic source imaging results for the serrated trailing edge with and without streamwise vanes at 4 kHz and 8 kHz frequencies are shown in Fig. 7. The source imaging results suggest that the noise is mainly emitted from the trailing edge of the wings. When serration is treated with streamwise vanes, they produce levels that are 3–4 dB lower than those of untreated serration at both frequencies.

The effectiveness of streamwise vanes in reducing serration noise at different angles of attack is illustrated in Fig. 8. It is noteworthy that the spectra below 800 Hz are impacted by unwanted background noise generated by the wind tunnel. Despite this, the results clearly demonstrate the effect of streamwise vanes in mitigating the high frequencies' broadband noise at zero and positive angles of attack. Notably, at a negative angle of attack of $\alpha = -5^\circ$, the untreated flapped serration is just 2.5 dB noisier than the corresponding non-flapped case, as shown in Fig. 8(a). This refers to a weaker cross-flow across serration since the positive flap angle counters the adverse flow generated due to negative angle of attack. Interestingly, the streamwise vanes are ineffective in reducing noise in this case.

At $\alpha = 0^\circ$, the non-flapped untreated serration demonstrates a significant reduction in trailing edge noise, with a reduction of up to 7 dB at high frequencies. However, the effectiveness of the serration noise reduction diminishes notably when the serration is at a flap angle of $\phi = 7^\circ$, as shown in Fig. 8(b). The observed increase in high-frequency noise with an increase in flap angle can be attributed to the

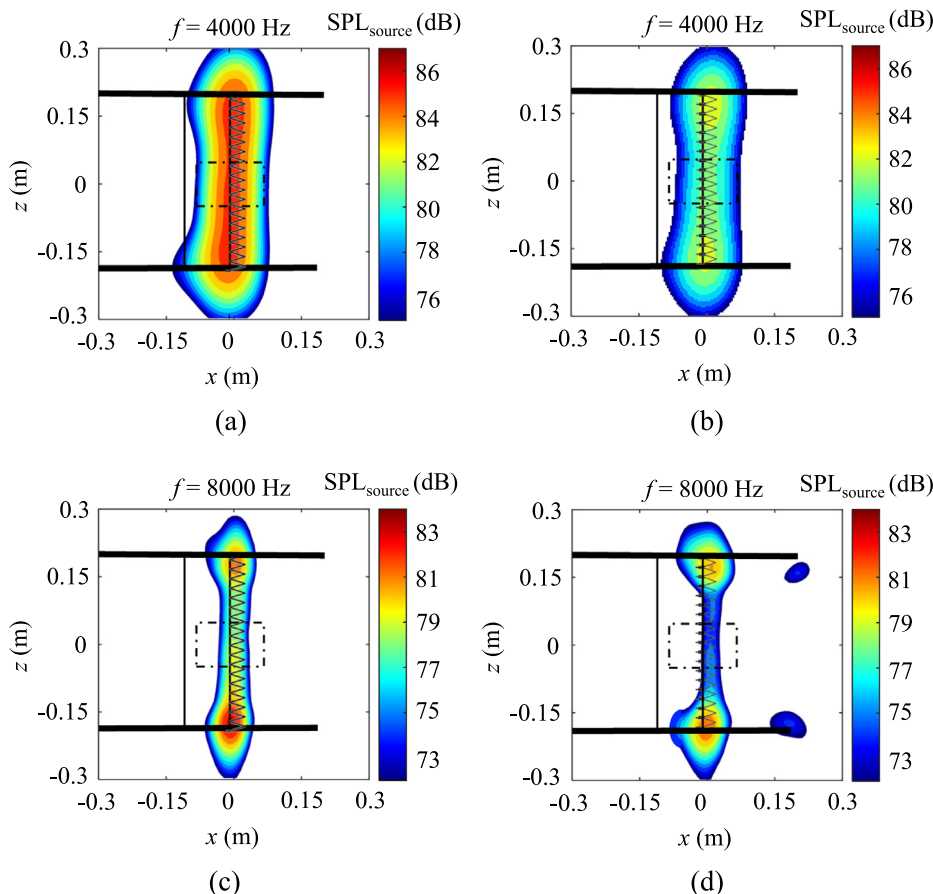


FIG. 7. (Color online) Source imaging results of the serrated trailing edge without (a), (c) and with C0 treatment (b), (d) at 40 m/s and $\alpha = 0^\circ$. The black rectangle in the center represents the wing. The two thick black horizontal lines represent the end plates. The black dashed-dotted rectangle in the center represents the source integration region.

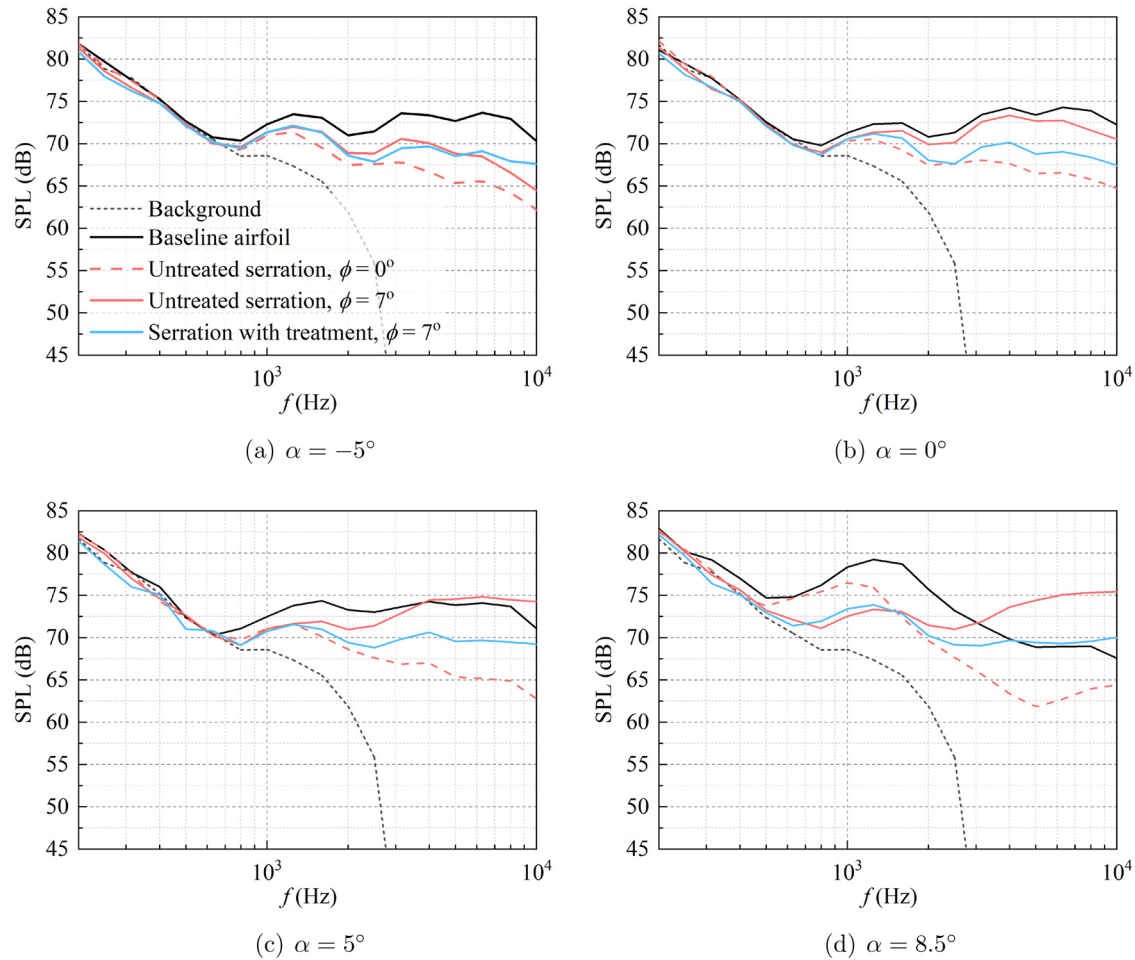


FIG. 8. (Color online) One-third octave trailing edge noise spectra showing the effect of the streamwise vane treatment (config. C0) on the flapped serration at 30 m/s.

cross-flow interacting with the serrations, as explained by Arce León *et al.*¹¹ The streamwise vane treatment when applied at the root of the flapped serration effectively reduces the broadband noise up to 3 dB at frequencies above 2 kHz. Additionally, the treatment remains equally effective at higher angle of attack. The treatment consistently achieves a significant broadband noise reduction of 5 dB above 3 kHz at both $\alpha = 5^\circ$ and $\alpha = 8.5^\circ$.

If the treatment reduces the cross-flow, it will be reasonable to infer that the frequency range where the treatment is effective coincides with the range where cross-flow is most prominent. Figure 9 compares the acoustic benefits of the treatment $\Delta\text{SPL}_{\text{treat.}} = \text{SPL}_{\text{w/o treat.}} - \text{SPL}_{\text{treat.}}$ with the contribution of the cross-flow, expressed as $\Delta\text{SPL}_{\text{cross-flow}} = \text{SPL}_{\phi=7^\circ} - \text{SPL}_{\phi=0^\circ}$ at different speeds, where $\Delta\text{SPL}_{\text{treat.}}$ is the change in sound pressure level (SPL) with treatment and $\text{SPL}_{\text{w/o treat.}}$ is the SPL without treatment. The frequency is normalised by the boundary layer thickness measured at the trailing edge, δ , and the free stream velocity, U_∞ . As shown in the figure, the profiles of $\Delta\text{SPL}_{\text{cross-flow}}$ at various speeds collapse well, indicating that the cross-flow has a dominant impact on noise in the frequency range where $f\delta/U_\infty > 0.15$. Notably, the treatment's effectiveness is observed in the same frequency range, which supports the hypothesis that it works by reducing cross-flow. The

deviation of $\Delta\text{SPL}_{\text{cross-flow}}$ and $\Delta\text{SPL}_{\text{treat.}}$ at $f\delta/U_\infty > 0.7$ is possibly caused by the extra noise related to the small-scale turbulent structures emerging from the streamwise vanes. However, further investigation is necessary to quantify this effect. To visualise the impact of the treatment on the cross-flow and understand the noise reduction mechanism, the flow results are presented in Sec. III B.

2. Effect of treatment position

To better understand the mechanism of noise reduction, a study was conducted in which the treatment was applied at various locations along the serration edges. Specifically, four different positions were tested: the root (configuration [config.] C3), middle (config. C7), tip (config. C8), and full serration (config. C9). The ΔSPL s between the treated and untreated serrations for each of these cases are plotted in Fig. 10. The results show that the treatment yields the highest noise reduction effectiveness when applied at the root of the serration. Applying the treatment at the middle position did not yield a substantial change in the noise level. However, when the treatment is applied near the tip, an undesired increase in noise is observed, indicating that treatments further away from the serration root may be less effective. Finally, the combination of all three treatments in

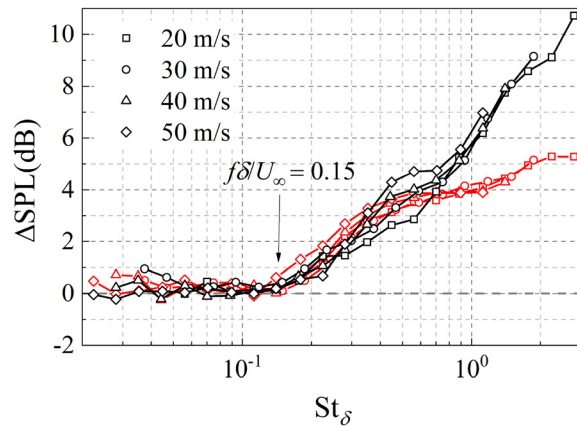


FIG. 9. (Color online) Comparison of $\Delta\text{SPL}_{\text{treat}} = \text{SPL}_{\text{w/o treat}} - \text{SPL}_{\text{treat}}$ (red line) and $\Delta\text{SPL}_{\text{cross-flow}} = \text{SPL}_{\phi=7^\circ} - \text{SPL}_{\phi=0^\circ}$ (black line) at $\alpha = 0^\circ$. A positive ΔSPL refers to noise reduction.

the fourth treatment configuration shows negligible reduction in noise.

Given that the cross-flow is most prominent near the serration root, as noted in Romani *et al.*,¹⁴ it is logical to position the treatment at the root of the serration to effectively counter the cross-flow. When the treatment is located away from the roots, it has diminished effect on the cross-flow. In addition, the wake from the treatment is expected to interact with the serration edges, resulting in an increase in noise. In case of the full serration, the positive impact of decreasing cross-flow is countered by the adverse interaction between the wake of the treatment and the serration edges. Thus, the full serration is observed to be ineffective in reducing noise.

B. Flow measurement

This section provides both hotwire and PIV results to better understand the noise reduction mechanism of the streamwise vanes. The hotwire measurements provide an overall flow field in the cross-flow plane downstream of the serration, whereas the PIV data focus on the flow from the

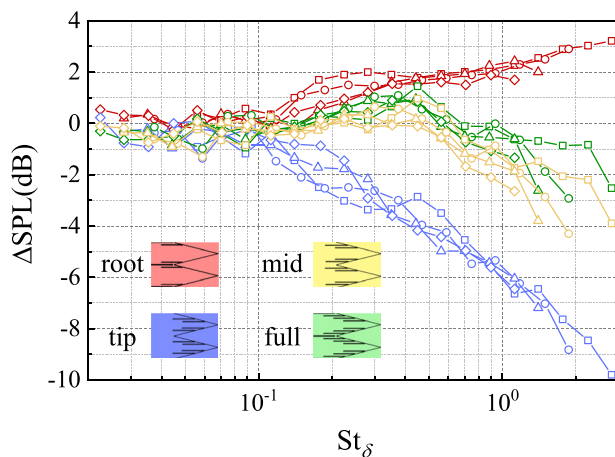


FIG. 10. (Color online) Comparison of ΔSPL between the treated and untreated serrations for different configurations: C3-root, C7-mid, C8-tip, and C9-full representing various treatment positions at $\alpha = 0^\circ$. A positive ΔSPL refers to noise reduction.

root of serration. The results for the serration cases with and without C0 treatment are compared.

First, the streamwise mean flow along the serration roots obtained from the PIV data is plotted in conjunction with streamlines in Fig. 11. Without treatment, the flapped serration exhibits a downward cross-flow through the serration valley, caused by the pressure gradient between the pressure and suction side. In contrast, with treatment, the flow becomes more aligned with the chord, indicating that the treatment helps to negate the adverse flow deflection observed with the cross-flow. Also, as the flow passes through these vanes, \bar{u}/U_∞ is reduced downstream of the treatment.

Furthermore, in order to examine the influence of the treatment on the overall serration flow, the mean flow in the cross-flow plane at $x/2h = 1.05$ measured by the hotwire is plotted in Fig. 12. In the figure, round symbols mark the tip of the serration, while the cross symbols mark the root of the serration. In the case of the untreated serration, there is an observable downward shift of the mean flow along the roots due to cross-flow. However, treatment results in a decrease in magnitude of the mean flow and an upward shift towards the roots, effectively counteracting the impact of the cross-flow.

The presence of cross-flow can be noticed in the wall-normal mean velocity (normal to the airfoil), as it induces streamwise counter-rotating vortex pairs across the serration, resulting in a strong upwash motion within the serration valley.¹¹ In Fig. 13, the contour of the \bar{v}/U_∞ along the serration root is plotted. For the untreated serration, a region of strong negative \bar{v}/U_∞ is visible on the suction side, originating downstream of the serration root. This indicates the presence of the cross-flow across the serration. After treatment, a notable decrease in \bar{v}/U_∞ is apparent on the suction side, suggesting a reduction in the cross-flow. Here, the streamwise vanes operate on a mechanism similar to winglets, which are commonly used to mitigate wing tip vortices. The vanes act as a barrier to reduce the airflow from the pressure side to the suction side through the gaps near the root of serrations.

Arce León *et al.*¹¹ found that a strong cross-flow results in a significant increase in the turbulent fluctuations downstream of the serration root. In order to establish a correlation between the observed high-frequency noise reduction above the Strouhal number, $St_\delta = 0.15$, and the velocity fluctuations, the velocity fluctuations obtained from both PIV and hotwire measurements were high-pass filtered to exclude values below this Strouhal number. Figure 14 presents the contours of the filtered normalised streamwise velocity fluctuations, u'_{RMS}/U_∞ , for both treated and untreated cases. The untreated serration exhibits enhanced fluctuations downstream of the root on the suction side, indicating a region of strong turbulence due to cross-flow. After treatment, these fluctuations are diminished, resulting in a more favourable flow field. The measurements obtained from the hotwire on the cross-flow plane confirm this observation, indicating that the treatment slightly diminishes the fluctuations in the vicinity of the root, while also causing an observable upward shift in the flow, as shown in Fig. 15. However, the fluctuations near the tip remain unaffected by the treatment.

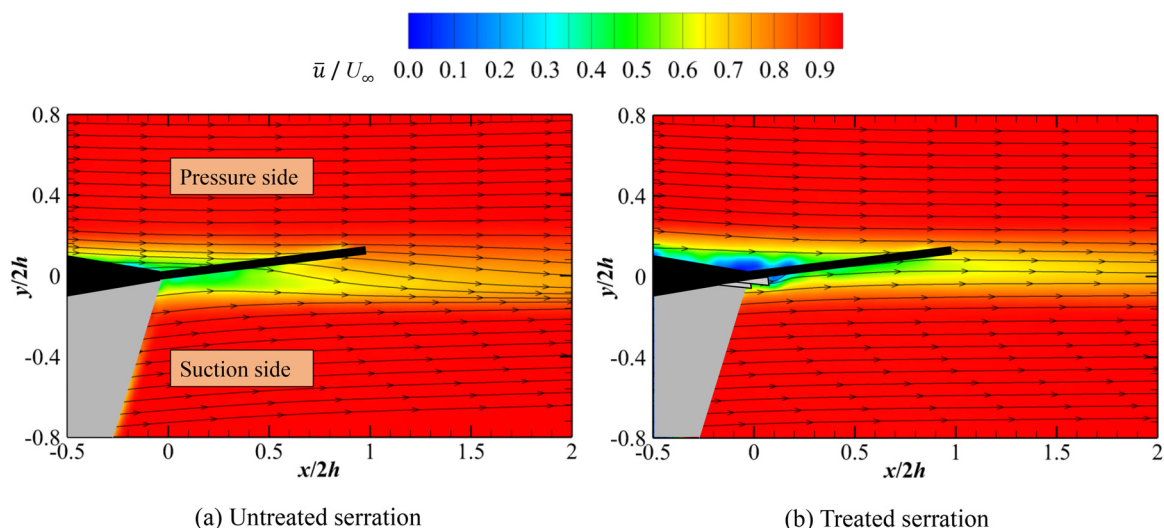


FIG. 11. (Color online) Contours of the mean streamwise velocity along with the streamlines obtained from PIV in the wall normal plane at $z/\lambda = 0$ for the flapped serration with and without C0 treatment at $\alpha = 0^\circ$ and 30 m/s.

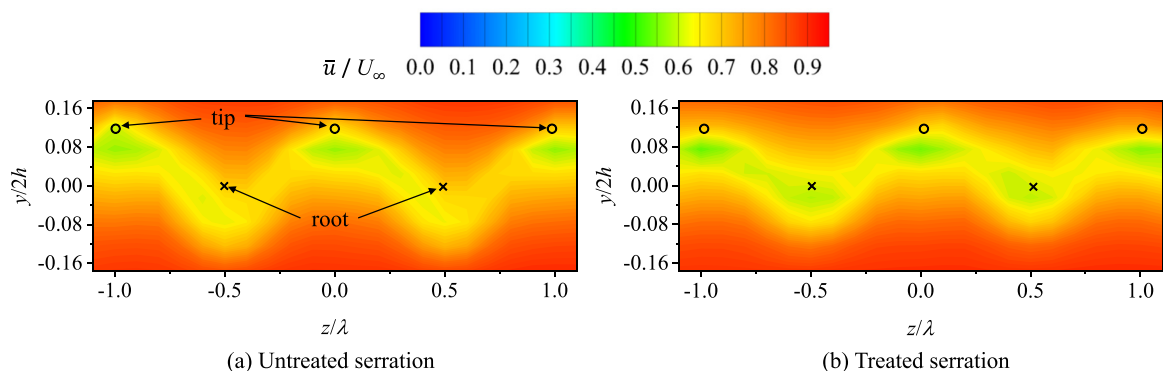


FIG. 12. (Color online) Contours of the mean streamwise velocity measured by hotwire in the cross-flow plane at $x/2h = 1.05$ for the flapped serration with and without C0 treatment at $\alpha = 0^\circ$ and 30 m/s.

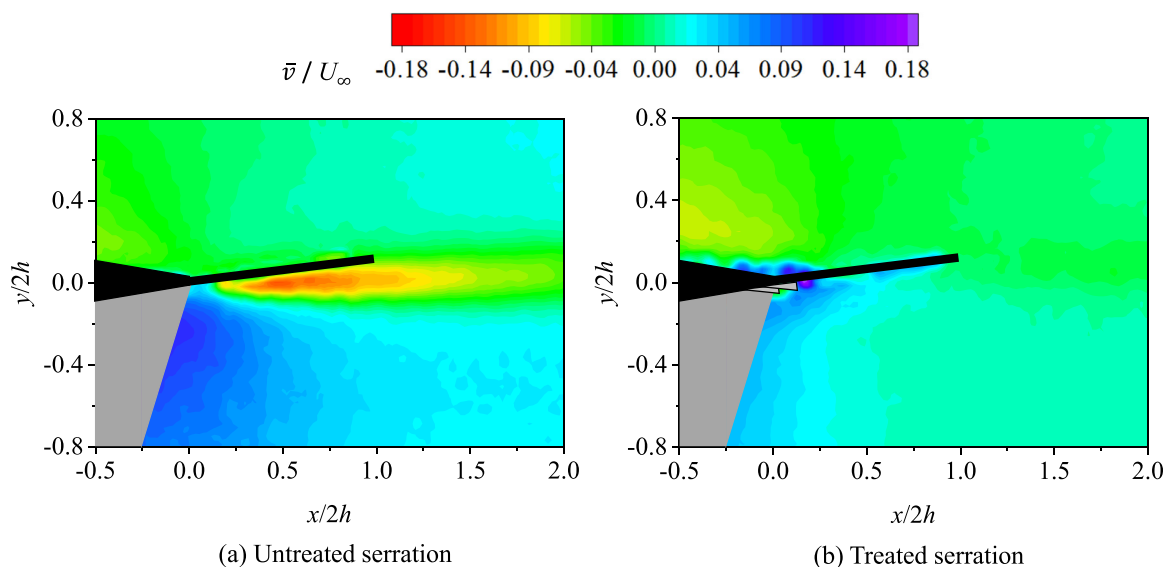


FIG. 13. (Color online) Contours of the mean velocity normal to the inflow obtained from PIV in the wall-normal plane at $z/\lambda = 0$ for the flapped serration ($\phi = 7^\circ$) with and without C0 treatment at $\alpha = 0^\circ$ and 30 m/s.

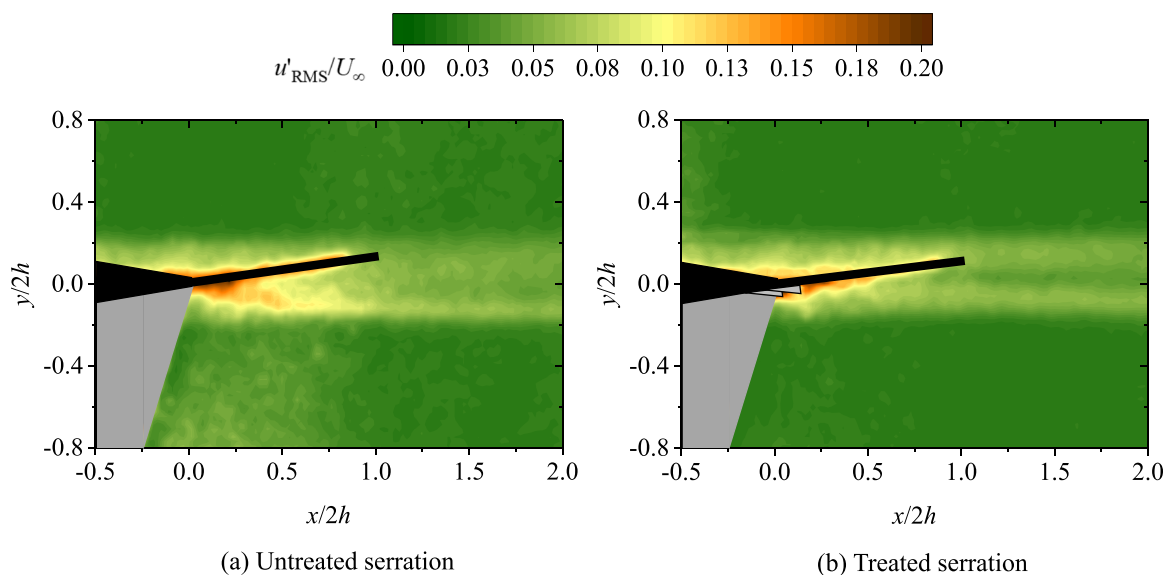


FIG. 14. (Color online) $u'_{\text{RMS}}/U_{\infty}$ distributions on wall-normal plane at $z/\lambda = 0$ obtained from PIV for the flapped serration ($\phi = 7^\circ$) with and without C0 treatment at $\alpha = 0^\circ$ and 30 m/s.

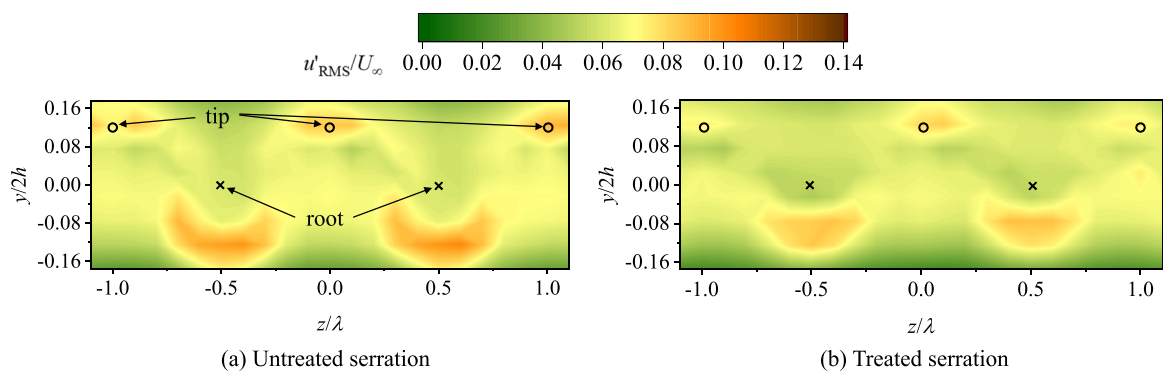


FIG. 15. (Color online) $u'_{\text{RMS}}/U_{\infty}$ distributions on the cross-flow plane at $x/2h = 1.05$ obtained from hotwire for the flapped serration $\phi = 7^\circ$ with and without C0 treatment at $\alpha = 0^\circ$ and 30 m/s.

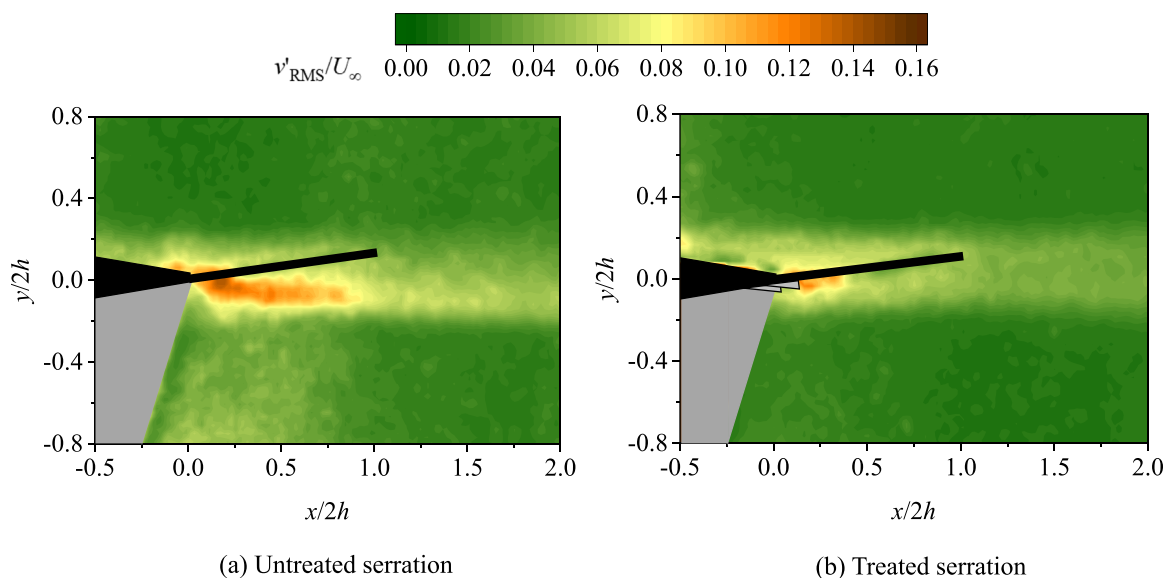


FIG. 16. (Color online) $v'_{\text{RMS}}/U_{\infty}$ distributions on the wall-normal plane at $z/\lambda = 0$ for the flapped serration ($\phi = 7^\circ$) with and without C0 treatment at $\alpha = 0^\circ$ and 30 m/s.

Furthermore, the contours of the normalised high-pass filtered wall-normal velocity fluctuations $v'_{\text{RMS}}/U_{\infty}$ at $z/\lambda = 0$ are shown in Fig. 16. Similar to the results for streamwise fluctuations, the $v'_{\text{RMS}}/U_{\infty}$ values for the untreated serration are enhanced at the suction side due to the cross-flow. However, with the treatment, a substantial reduction in $v'_{\text{RMS}}/U_{\infty}$ can be observed downstream of the root on the suction side. The presence of $v'_{\text{RMS}}/U_{\infty}$ near the serrations and their proximity to the sharp edge indicates their contribution to the far-field noise.^{16,30} Thus, the observed decrease in noise emissions resulting from the treated serrations aligns well with the lower values of $v'_{\text{RMS}}/U_{\infty}$ detected in these cases.

The analysis above has deepened our understanding of how to effectively address cross-flow and improve the noise reduction performance of the trailing edge serrations using streamwise vane treatments. For the untreated serrations, the noise reduction performance is highly sensitive to the misalignment with the flow.^{11,31} The variation in angles of attack or manufacturing errors makes it hard to avoid flow misalignment under all conditions. Fortunately, adding streamwise vanes at the root of the serration is a promising practical solution.

C. Load measurement

The practical implementation of the streamwise vane treatment requires careful consideration of its impact on the aerodynamic performance. In this section, the effect of streamwise vanes on the aerodynamic loading of the $\phi = 7^\circ$ serrated wing model is analyzed. For all cases, the planform area of the wing model without serrations was used for the calculation of lift coefficients (Cl) and drag coefficients (Cd). Figure 17(a) shows the lift and drag coefficients of different configurations as a function of angle of attack, and the changes in Cl and Cd caused by streamwise vanes are shown in Fig. 17(b). In the pre-stall region, the streamwise vanes did not cause noticeable variation in the lift coefficient, but led to consistent increase in the drag coefficient, which can be attributed to the additional skin friction drag and pressure drag caused by the vanes. The drag increase is less than 6% for positive angles of attack, and the relative drag penalty reduces as the angle of attack increases. Furthermore, Fig. 17(c) indicates that the streamwise vanes lead to a less than 5% reduction in the lift-to-drag ratio.

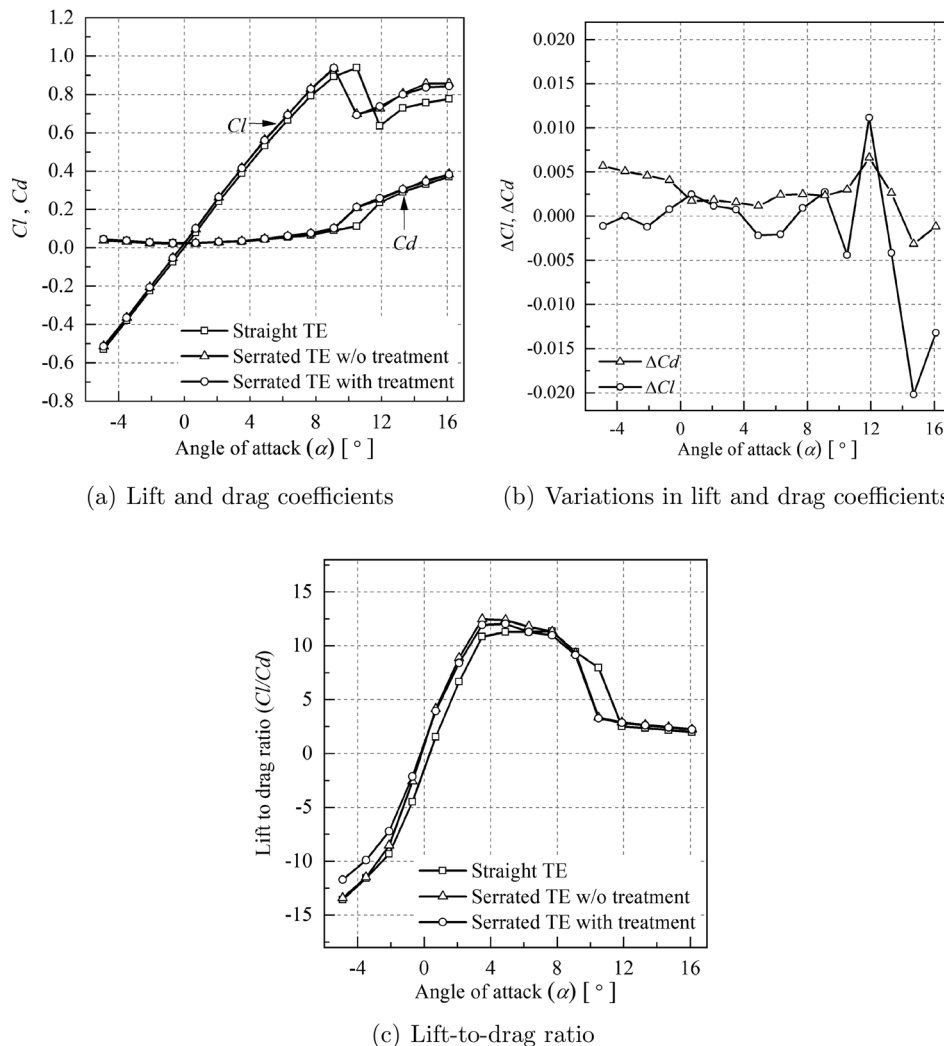


FIG. 17. The aerodynamic performance of the baseline wing model and the model with different treatments: (a) lift and drag coefficients, (b) the change in the lift and drag coefficients by the streamwise vanes (i.e., the difference between “Serrated TE with treatment” and “Serrated TE w/o treatment,” respectively), and (c) the lift-to-drag ratio. Measurements were taken at $U_{\infty} = 30$ m/s.

IV. CONCLUSION

The study aims to enhance the performance of the trailing edge serration at incidence by adding streamwise vane treatment. A NACA 0012 wing model attached with sawtooth type serrations was used for the study. Acoustic measurements were conducted using a phased microphone array. The results reveal that the streamwise vane treatment is effective in reducing aerodynamic noise in the mid- to high-frequency range for the flapped serrations when placed at the root. However, relocating the treatment towards the tip of the serration showed an adverse impact on noise. The PIV results of the treatment at the root reveal a substantial reduction in cross-flow after treatment. The treatment successfully reduces the root flow turbulence kinetic energy (TKE) and the streamwise and wall-normal fluctuations in the serration valley. Importantly, the treatment did not compromise the aerodynamic performance of the wing model. Overall, this study provides compelling evidence of the potential of streamwise treatments applied at the root of serrations for enhancing their noise-reducing capabilities, particularly in the presence of flow misalignment. The implications of the treatments and connection between the flow and noise measurements are comprehensively investigated.

ACKNOWLEDGMENTS

This work is supported by the Hong Kong Research Council (RGC 16204721).

AUTHOR DECLARATIONS

Conflict of Interest

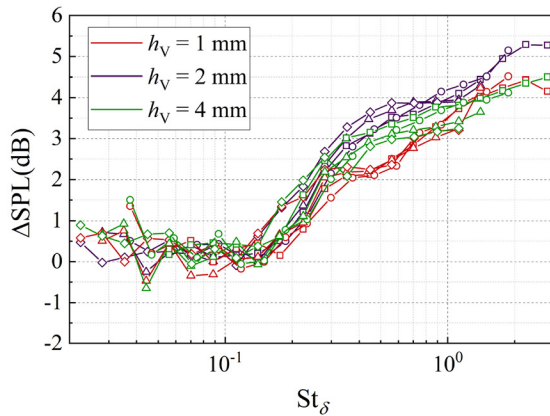
The authors have no conflicts to disclose.

DATA AVAILABILITY

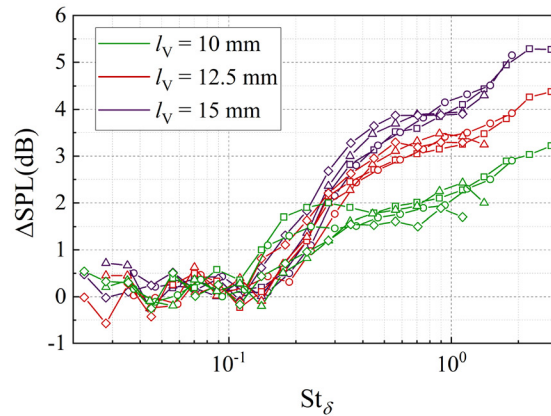
The data that support the findings of this study are available within the article.

APPENDIX: PARAMETRIC STUDY OF THE STREAMWISE VANES

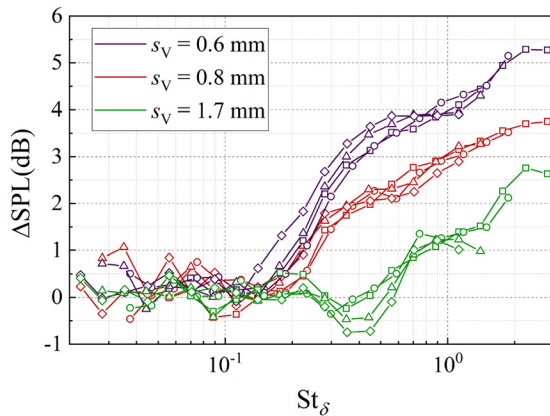
A parametric study was conducted to determine the optimal height, length, and spacing of streamwise vanes for maximum noise reduction. The results of this study are presented in this section. Figure 18(a) shows a comparison of the noise reduction observed by the streamwise vanes of different heights (configurations C0, C1, and C2).



(a) Variation of height: Config. C0, C1, C2



(b) Variation of length: Config. C0, C3, C4



(c) Variation of spacing: Config. C0, C5, C6

FIG. 18. (Color online) Effect of various streamwise vanes parameters on the noise reduction at flow speeds of 20 m/s (\square), 30 m/s (\circ), 40 m/s (\triangle), and 50 m/s (\diamond). Positive Δ SPL denotes noise reduction.

The height is varied from $h_v = 1\text{--}4\text{ mm}$, corresponding to $h_v/\delta \approx 0.25\text{--}1$. As shown in the figure, the noise reduction increases with height up to 2 mm ($h_v/\delta \approx 0.5$). With further increase in height to 4 mm ($h_v/\delta \approx 1$), no further improvement in the noise reduction is observed.

Furthermore, Fig. 18(b) illustrates the impact of varying streamwise vane length on noise reduction performance by comparing configurations C0, C3, and C4. The results demonstrate a clear correlation between vane length and noise reduction, with longer vanes providing greater noise reduction. The optimal length for maximum noise reduction is $l_v = 15\text{ mm}$, corresponding to $l_v/h_v = 7.5$. Increasing the length allows for greater flow development through the vanes, thus slowing down the flow as it passes through them.

Finally, the impact of streamwise vane spacing on noise reduction performance is presented in Fig. 18(c). Three different configurations, C0, C5, and C6, with vane spacings of $s_v = 0.6\text{ mm}$, 0.8 mm , and 1.2 mm , respectively are considered for the study. The results indicate that noise reduction improves as spacing is decreased. The minimum spacing of $s_v = 0.6\text{ mm}$ provides the best noise reduction performance. The parametric analysis reveals that vane spacing has a greater impact on noise reduction than vane height and length.

- ¹M. Gruber, P. Joseph, and T. Chong, "On the mechanisms of serrated airfoil trailing edge noise reduction," in *17th AIAA/CEAS Aeroacoustics Conference (32nd AIAA Aeronautics Conference)*, Portland, OR (June 5–8, 2011), AIAA Paper AIAA2011-2781.
- ²P. Zhou, S. Zhong, X. Li, Y. Li, W. Chen, H. Jiang, and X. Zhang, "Broadband trailing edge noise reduction through porous velvet-coated serrations," *Phys. Fluids* **34**(5), 057112 (2022).
- ³T. F. Geyer and E. Sarraj, "Trailing edge noise of partially porous airfoils," in *20th AIAA/CEAS Aeroacoustics Conference*, Atlanta, GA (June 16–20, 2014), AIAA paper 2014-3039.
- ⁴I. A. Clark, W. N. Alexander, W. Devenport, S. Glegg, J. W. Jaworski, C. Daly, and N. Peake, "Bioinspired trailing-edge noise control," *AIAA J.* **55**(3), 740–754 (2017).
- ⁵F. Gstrein, B. Zang, Y. D. Mayer, and M. Azarpeyvand, "Airfoil trailing-edge noise reduction by application of finlets," *AIAA J.* **60**(1), 1–248 (2021).
- ⁶N. Nurani Hari, M. Szoke, W. J. Devenport, and S. A. Glegg, "Understanding pressure shielding by canopies," in *AIAA Scitech 2021 Forum* (January 11–15 and 19–21, 2021), AIAA Paper 2021-0817.
- ⁷S. Oerlemans, "Reduction of wind turbine noise using blade trailing edge devices," in *22nd AIAA/CEAS Aeroacoustics Conference*, Lyon, France (May 30–June 1, 2016), AIAA Paper 2016-3018.
- ⁸S. Oerlemans, M. Fisher, T. Maeder, and K. Kögler, "Reduction of wind turbine noise using optimized airfoils and trailing-edge serrations," *AIAA J.* **47**(6), 1470–1481 (2009).
- ⁹F. Avallone, S. Pröbsting, and D. Ragni, "Three-dimensional flow field over a trailing-edge serration and implications on broadband noise," *Phys. Fluids* **28**(11), 117101 (2016).
- ¹⁰T. P. Chong and A. Vathylakis, "On the aeroacoustic and flow structures developed on a flat plate with a serrated sawtooth trailing edge," *J. Sound Vib.* **354**, 65–90 (2015).
- ¹¹C. Arce León, D. Ragni, S. Pröbsting, F. Scarano, and J. Madsen, "Flow topology and acoustic emissions of trailing edge serrations at incidence," *Exp. Fluids* **57**(5), 1–17 (2016).

- ¹²A. Vathylakis, C. C. Paruchuri, T. P. Chong, and P. Joseph, "Sensitivity of aerofoil self-noise reductions to serration flap angles," in *22nd AIAA/CEAS Aeroacoustics Conference*, Lyon, France (May 30–June 1, 2016), AIAA Paper 2016-2837.
- ¹³P. C. Woodhead, T. P. Chong, and J. Wissink, "Exploiting the misalignment of the serrated trailing edge for improved aerofoil broadband noise reduction," in *23rd AIAA/CEAS Aeroacoustics Conference*, Denver, CO (June 5–9, 2017), AIAA Paper 2017-4175.
- ¹⁴G. Romani, D. Casalino, and W. van der Velden, "Numerical analysis of airfoil trailing-edge noise for straight and serrated edges at incidence," *AIAA J.* **59**(7), 2558–2577 (2021).
- ¹⁵P. Woodhead, T. Chong, P. Joseph, and A. Vathylakis, "Aerofoil self-noise radiations subjected to serration flap angles," *Exp. Fluids* **62**(7), 1–22 (2021).
- ¹⁶M. S. Howe, "Noise produced by a sawtooth trailing edge," *J. Acoust. Soc. Am.* **90**(1), 482–487 (1991).
- ¹⁷L. T. L. Pereira, D. Ragni, F. Avallone, and F. Scarano, "Aeroacoustics of sawtooth trailing-edge serrations under aerodynamic loading," *J. Sound Vib.* **537**, 117202 (2022).
- ¹⁸S. Sundeep, P. Zhou, and S. Zhong, "Enhancing the noise reduction capability of the trailing edge serration at incidence," in *52nd International Congress and Exposition on Noise Control Engineering, INTER-NOISE 2023*, Chiba, Japan (2023).
- ¹⁹Y. Shi and W. Kollmann, "Wall-modeled large-eddy simulation of a trailing-edge serration-finlet configuration," *AIP Adv.* **11**(6), 065222 (2021).
- ²⁰A. Afshari, M. Azarpeyvand, A. A. Dehghan, and M. Szoke, "Effects of streamwise surface treatments on trailing edge noise reduction," in *23rd AIAA/CEAS Aeroacoustics Conference*, Denver, CO (June 5–9, 2017), AIAA Paper 2017-3499.
- ²¹W. Yi, P. Zhou, Y. Fang, J. Guo, S. Zhong, X. Zhang, X. Huang, G. Zhou, and B. Chen, "Design and characterization of a multifunctional low-speed anechoic wind tunnel at HKUST," *Aerosp. Sci. Technol.* **115**, 106814 (2021).
- ²²I. H. Abbott, A. E. Von Doenhoff, and L. Stivers, Jr., "Summary of airfoil data" (NACA-TR-824, 1945).
- ²³T. Brooks, M. Marcolini, and D. Pope, "Airfoil trailing edge flow measurements and comparison with theory, incorporating open wind tunnel corrections," in *9th Aeroacoustics Conference*, Williamsburg, VA (October 10–15, 1984), AIAA Paper 84-2266.
- ²⁴W. K. Blake, *Mechanics of Flow-Induced Sound and Vibration, Vol. 2: Complex Flow-Structure Interactions* (Academic Press, Cambridge, MA, 2017).
- ²⁵D. H. Johnson and D. E. Dudgeon, *Array Signal Processing: Concepts and Techniques* (Prentice-Hall, Hoboken, NJ, 1993).
- ²⁶T. Brooks and W. Humphreys, Jr., "Effect of directional array size on the measurement of airframe noise components," in *5th AIAA/CEAS Aeroacoustics Conference and Exhibit*, Bellevue, WA (May 10–12, 1999), AIAA Paper 99-1958.
- ²⁷R. Merino-Martínez, S. Luesutthiviboon, R. Zamponi, A. R. Carpio, D. Ragni, P. Sijtsma, M. Snellen, and C. Schram, "Assessment of the accuracy of microphone array methods for aeroacoustic measurements," *J. Sound Vib.* **470**, 115176 (2020).
- ²⁸P. Zhou, S. Zhong, and X. Zhang, "On the effect of velvet structures on trailing edge noise: Experimental investigation and theoretical analysis," *J. Fluid Mech.* **919**, A11 (2021).
- ²⁹F. Champagnat, A. Plyer, G. Le Besnerais, B. Leclaire, S. Davoust, and Y. Le Sant, "Fast and accurate PIV computation using highly parallel iterative correlation maximization," *Exp. Fluids* **50**(4), 1169–1182 (2011).
- ³⁰R. K. Amiet, "Noise due to turbulent flow past a trailing edge," *J. Sound Vib.* **47**(3), 387–393 (1976).
- ³¹C. Arce León, R. Merino-Martínez, D. Ragni, F. Avallone, F. Scarano, S. Pröbsting, M. Snellen, D. G. Simons, and J. Madsen, "Effect of trailing edge serration-flow misalignment on airfoil noise emissions," *J. Sound Vib.* **405**, 19–33 (2017).